Can Australian Multiyear Droughts and Wet Spells Be Generated in the Absence of Oceanic Variability?

ANDRÉA S. TASCHETTO AND ALEX SEN GUPTA

Climate Change Research Centre, and ARC Centre of Excellence for Climate System Science, University of New South Wales, Sydney, New South Wales, Australia

CAROLINE C. UMMENHOFER

Department of Physical Oceanography, Woods Hole Oceanographic Institution, Woods Hole, Massachusetts

MATTHEW H. ENGLAND

Climate Change Research Centre, and ARC Centre of Excellence for Climate System Science, University of New South Wales, Sydney, New South Wales, Australia

(Manuscript received 1 October 2015, in final form 28 April 2016)

ABSTRACT

Anomalous conditions in the tropical oceans, such as those related to El Niño–Southern Oscillation and the Indian Ocean dipole, have been previously blamed for extended droughts and wet periods in Australia. Yet the extent to which Australian wet and dry spells can be driven by internal atmospheric variability remains unclear. Natural variability experiments are examined to determine whether prolonged extreme wet and dry periods can arise from internal atmospheric and land variability alone. Results reveal that this is indeed the case; however, these dry and wet events are found to be less severe than in simulations incorporating coupled oceanic variability. Overall, ocean feedback processes increase the magnitude of Australian rainfall variability by about 30% and give rise to more spatially coherent rainfall impacts. Over mainland Australia, ocean interactions lead to more frequent extreme events, particularly during the rainy season. Over Tasmania, in contrast, ocean–atmosphere coupling increases mean rainfall throughout the year. While ocean variability makes Australian rainfall anomalies more severe, droughts and wet spells of duration longer than three years are equally likely to occur in both atmospheric- and ocean-driven simulations. Moreover, they are essentially indistinguishable from what one expects from a Gaussian white noise distribution. Internal atmosphere–land-driven megadroughts and megapluvials that last as long as ocean-driven events are also identified in the simulations. This suggests that oceanic variability may be less important than previously assumed for the long-term persistence of Australian rainfall anomalies. This poses a challenge to accurate prediction of long-term dry and wet spells for Australia.

1. Introduction

Australia's climate is characterized by high temporal and spatial variability (Nicholls et al. 1997). Extreme events range in spatial extent and time scale, from multiyear, continental-scale droughts to localized flash floods. Severe droughts have widespread social and economic consequences for agriculture, ecosystems, and human welfare. For instance, Australia suffered dramatic crop and livestock losses during the Federation Drought from 1895 to 1902, the World War II Drought from 1937 to 1945, and the more recent Millennium Drought (or Big Dry) from 1995 to 2009 (Verdon-Kidd and Kiem 2009). Extreme wet events can also have a devastating impact for the nation—for example, the floods that affected many regions across the continent during the ''Big Wet'' in 1974 and also during 2010–12. Figure 1 summarizes the driest and wettest eras in Australia using the 1900–2014 Australian Water Availability Project (AWAP) rainfall dataset (Raupach et al. 2009).

Corresponding author address: Andréa S. Taschetto, Climate Change Research Centre, UNSW Australia, Sydney NSW 2052, Australia.
E-mail: a.taschetto@unsw.edu.au

DOI: 10.1175/JCLI-D-15-0694.1

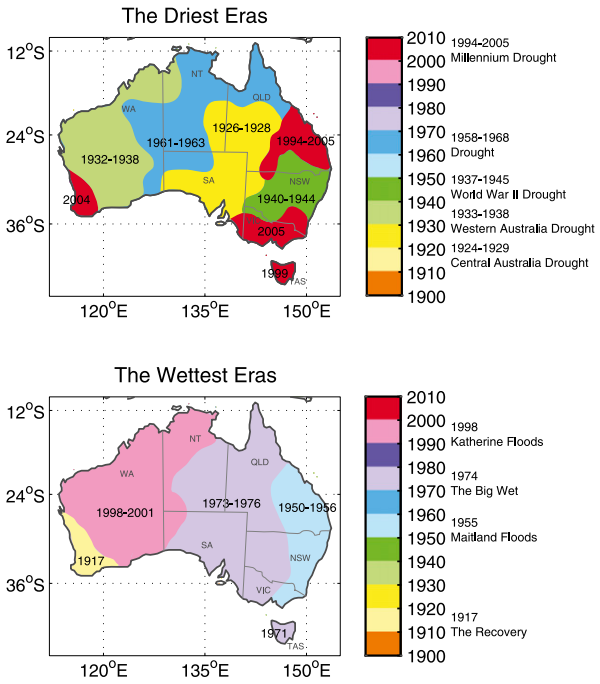

FIG. 1. Schematic of (top) era of driest decade and (bottom) era of wettest decade. Annual mean rainfall anomalies are constructed from monthly anomalies based on the AWAP rainfall dataset from 1900 to 2014. To avoid influences of data errors or localized rainfall extreme events, a spatial linear filter was applied to obtain a consistent smooth large-scale pattern over Australia. The wettest or driest periods indicated in the schematic were then selected by choosing the maximum and minimum rainfall anomaly of the 11-yr running mean time series for each grid point. Areas are colored to indicate grid points within the same decade, and the years represent the center of the anomalous events. Some of the extensive droughts and extreme wet events are indicated on the right side of the color bar. The largest Australian political divisions are also indicated: Western Australia (WA), Northern Territory (NT), South Australia (SA), Queensland (QLD), New South Wales (NSW), Victoria (VIC), and Tasmania (TAS).

After the rainfall deficits of the Federation Drought, many parts of central and South Australia experienced intense dry conditions during 1926–28 (Fig. 1, top). Australia again suffered widespread drought over the western half of the continent in the 1930s and over large parts of eastern Australia in the first half of the 1940s (Fig. 1, top) during the World War II Drought, also known as the Forties Drought (Verdon-Kidd and Kiem 2009). Dry conditions affected the Northern Territory and Australian interior in the early 1960s (Fig. 1, top).

In 1982, New South Wales and Victoria were affected by the worst short-term drought since the beginning of the century driven by the strong 1982 El Niño event. In the early 1990s, parts of northern Australia experienced dry conditions that were intensified in 1994/95, especially over Queensland (Fig. 1, top), by a series of weak El Niño events. This dry spell marked the beginning of the so-called Millennium Drought that persisted into the early 2000s.

The Millennium Drought was widespread across much of the continent during 2002–06 and persisted much longer across localized regions over southeast Australia. The long duration of this dry spell has been associated with sea surface temperature (SST) conditions in the Indian and Pacific Oceans. Ummenhofer et al. (2009) show that the absence of negative Indian Ocean dipole (IOD) events during the Big Dry from 1995 to 2006, as well as during the Federation Drought in 1895–1903, reduced tropical moisture advection to southeastern Australia. In addition, during the Big Dry period, one of the worst short-term droughts was recorded in 2002 (Nicholls 2004), particularly intense in the southeast across Victoria (Fig. 1, top). Low rainfall rates were associated with a weak El Niño event in 2002 and exacerbated by high evaporation rates due to very high daytime temperatures (Karoly et al. 2003; Nicholls 2004). The drought continued for the following few years over eastern Australia, persisting until 2009 in some regions of Victoria (Gergis et al. 2012).

Long wet spells have also affected Australia's climate in significant and costly ways. An interesting feature of Fig. 1 (bottom) is that wet eras are coherent over more extensive regions than dry eras. The reason for this spatial asymmetry is unclear, but it is likely related to the asymmetric response of Australian rainfall to El Niño–Southern Oscillation (ENSO) events. In particular, Power et al. (2006) have shown that strong La Niña events are tightly linked to a large-scale Australian response, whereas the magnitude of El Niño events is a poorer predictor for the severity of Australia's dryness. This nonlinear response of rainfall intensity to ENSO may also apply to spatial scales. Here we will show that the spatial asymmetry between wet and dry spells is reproduced in a fully coupled climate model simulation.

At the beginning of the twentieth century, after the Federation Drought, parts of Western Australia experienced extreme wet conditions during the period known as "The Recovery" of 1915–17 (Fig. 1, bottom). The 1950–56 period was the wettest era over the east (Fig. 1b), when parts of NSW experienced recurrent floods over the Maitland region (BoM 2015a). The 1970s marked the wettest long-term period over large areas of Australia (Fig. 1, bottom). This unprecedented wet period, known as the Big Wet in 1974, was combined with flash floods in the east and an active cyclone season in 1974/75 (BoM 2015b). The late 1990s were exceptionally wet over Western Australia and the Northern Territory (Fig. 1, bottom), particularly because of very heavy rain events in the tropics during the recurrent La Niña

conditions from March 1998 to March 2001 (Okumura and Deser 2010).

More recently, Australia (on average) experienced the wettest 24-month period on record from April 2010 to March 2012. The reasons for this continental-scale wet spell are still under debate; however, it is likely a combination of a strong La Niña event and changes associated with a negative phase of the southern annular mode (SAM; Hendon et al. 2014; Lim et al. 2016) in addition to a long-term warming signal in the oceans (Ummenhofer et al. 2015). This recent anomalous wet period is not apparent in Fig. 1 (bottom) as that analysis highlights only decadal anomalies.

Many of the iconic large-scale droughts and pluvials in Australia are thought to be driven by anomalous equatorial Indo-Pacific SST—for example, the short 1982/83 and long 1991–95 El Niño–related droughts and the Big Wet associated with the persistent 1973–76 La Niña. Prolonged drought episodes in Australia's southeast and Murray–Darling River basin, such as the World War II and Millennium Droughts, were also linked to unusual Indian Ocean conditions (Ummenhofer et al. 2009, 2011). Variations in ocean temperatures on multidecadal time scales also cause drought conditions in Australia. For instance, Verdon-Kidd and Kiem (2009) associate the Federation Drought with sustained El Niño activity and a positive phase of the interdecadal Pacific oscillation (IPO). The IPO modulates the relationship between ENSO and Australian rainfall on interdecadal time scales, such that teleconnections are more robust during IPO negative phases (Power et al. 1999). Multidecadal drought periods, sometimes referred to as megadroughts, have been reported in North America via multicentury tree-ring reconstructions (Cook et al. 2007) and have been associated with a shift toward a La Niña–like mean state in the tropical Pacific (Coats et al. 2015). In Australia, mega-rainfall episodes over the past few centuries have received much less attention in the literature, although such events have been found in paleoreconstructions dating back 100 kyr (1 kyr = 1000 yr; e.g., Cohen et al. 2011, 2012a). In the past millennium, Cohen et al. (2012b) show evidence of a megapluvial episode in southern Australia driven by an anomalous sea level trough extending from the Southern Ocean into central Australia, resulting in Lake Callabonna filling to more than 10 times the volume of its largest historical filling in 1974. Megadroughts in Australia's past millennium have been recently identified by Vance et al. (2015); using a millennial-length IPO reconstruction, they suggest a close link between its positive phase and the occurrence of megadroughts in southeastern Australia (including one lasting 39 yr). Multiproxy reconstruction data by Gergis et al. (2012) suggest a robust relationship between variations in southeast Australia rainfall, ENSO, and IPO. In this study, we will show that Australian megadroughts and megapluvials can be simulated in multicentury simulations from a coupled climate model.

Variations of ocean temperatures are not the only factor affecting floods and droughts in Australia. For example, Kiem and Verdon-Kidd (2010) suggest that the SAM was a major driver of the Big Dry in southeast Australia. Cai et al. (2011) attributed the lowest winter rainfall in southwestern Western Australia in 2010 to a positive phase of the SAM. The SAM is an intrinsic mode of variability in the atmosphere characterized by variations in the position (latitude) and strength of the Southern Hemisphere midlatitude westerlies. The SAM has been shown to modulate precipitation over southwest Western Australia, Victoria, and Tasmania (Hendon et al. 2007; Hill et al. 2009). Although the SAM can impact southern high-latitude ocean and sea ice variability (Sen Gupta and England 2006), it is mainly associated with internal atmospheric variability and is largely unrelated to any localized feedback in oceanic conditions (Sen Gupta and England 2007). On multidecadal time scales greenhouse gases and ozone have been implicated in changing the SAM (Arblaster and Meehl 2006).

In cases where floods and droughts are caused by remote SST variability (e.g., associated with ENSO and the IOD), ocean memory provides potential forecast skill on seasonal time scales (e.g., Shukla et al. 2000; Meinke et al. 2005) and beyond (Meehl et al. 2014; Jourdain et al. 2016). In contrast, rainfall prediction due to atmospheric variability ranges from 1 month in case of low-frequency planetary waves (Shukla 1981) up to 4 months in the case of atmospheric oscillations such as the SAM (Seviour et al. 2014). There is relatively little forecasting skill beyond seasonal time scales, and even when this happens it is indirectly linked to oceanic conditions; for example, the seasonal predictability of SAM linked to ENSO reported by Lim et al. (2013). Moreover, Gallant et al. (2013) suggest that the relationships between ENSO and SAM and precipitation over Australia are nonstationary on multidecadal time scales, possibly forced by internal climate variability. Thus, predicting drought or flood characteristics at extended lead times is more challenging where ocean memory is not involved.

Sea surface temperature has been shown to provide high potential predictive skills for air temperature, precipitation, and sea level pressure over the tropics, although this decreases over certain significant land areas, such as Australia, parts of Africa, and South America (Manabe and Stouffer 1996; Rowell 1998;

Taschetto and Wainer 2008; Feng et al. 2011). In contrast, internal atmospheric variability dominates variations in the extratropical regions (Kushnir et al. 2002), making predictions more difficult. For instance, Power et al. (1995) demonstrate that stochastic variability becomes more important than variability associated with SST over the extratropics and that it can result in subsequent variability on decadal time scales unrelated to oceanic processes.

Previous studies using numerical models have suggested that stochastic atmospheric variability can play a significant role in the occurrence of megadroughts in certain regions of the globe—for example, North America (Coats et al. 2013a; Stevenson et al. 2015), India (Hunt 2012), and Australia (Hunt 2009; Gallant et al. 2013). If stochastic processes are the primary factor driving megadroughts and megapluvials, this compromises the predictability of extended periods of dry and wet episodes.

To better understand prediction limitations, it is important to understand the extent to which long-term dry and wet periods in Australia can be triggered and maintained without ocean memory. The goal of this study is to investigate the role of the ocean in modulating annual to multidecadal variability in rainfall and whether extended dry and wet periods are possible as a result of internal atmospheric and land surface variability alone. We use experiments within a coupled climate model to assess how prolonged dry and wet spells differ when ocean variability is suppressed. The model and numerical simulations are described in the next section. The simulated rainfall response to oceanic and atmospheric variability is examined in terms of mean and extremes in section 3. The spatial impact of droughts and wet spells is examined in section 4. Section 5 explores rainfall distribution in three regions in Australia and its variability via power spectrum and autocorrelation analyses. The severity, duration, and return period of extended dry and wet spells, as well as their seasonality, are evaluated in section 6. Section 7 presents a discussion of decadal variability and identifies internal atmosphere–land-driven and ocean-driven megadroughts and megapluvials in the model and associated mechanisms. Finally, discussion and conclusions are presented in the last two sections.

2. Methodology

To assess the role of internal atmospheric variability in driving long-term dry and wet spells over Australia, we use the NCAR Community Earth System Model, version 1.0.5 (CESM1.0.5; Gent et al. 2011), configured both 1) in fully coupled mode and 2) in atmospheric experiments. The configuration of the CESM used in this study consists of the following model components: atmosphere [Community Atmosphere Model, version 4 (CAM4)], sea ice [Community Ice Code, version 4 (CICE4)], land [Community Land Model, version 4 (CLM4)], and ocean [Parallel Ocean Program, version 2 (POP2)] as well as a coupling infrastructure (CPL7) that exchanges state information between them.

The two simulations are performed at a resolution of 1.9° latitude by 2.5° longitude for both atmosphere and ocean—a fully coupled simulation performed with the general circulation model (GCM) referred to as CPLD and an atmospheric GCM run, referred to as AGCM.

The CPLD simulation consists of a 700-yr integration. In this simulation, all components of the climate system fully interact with each other, and thus this run contains all forms of coupled variability, including coupled variability reliant on oceanic process, such as ENSO.

The AGCM simulation is integrated for 1000 yr and is forced with a repeating 12-month SST and sea ice climatology constructed from output of the CPLD simulation. As such, the monthly SST climatology is the same in both simulations, but the AGCM simulation has no interannual or longer time-scale variability in SST. In both experiments the land component is active and responds to the atmospheric fluxes.

In neither experiment did we impose any external forcings that could result in further decadal and/or multidecadal variability, such as solar forcing, volcanoes, aerosols, ozone depletion, or greenhouse gas increases. Therefore, any unforced component of decadal rainfall extremes arises as a result of internal atmosphere–land variability (AGCM) and/or coupled ocean–atmosphere–land–ice processes (CPLD).

By examining the difference between these two simulations we can determine whether internal variability in the atmosphere–land system is able to generate extended periods of dry or wet conditions as intense and/or persistent as those produced when coupling the atmosphere with the ocean. These experiments are not, of course, mutually exclusive in that regard; that is, internal atmospheric and land variability will be present in the CPLD experiments, as well as in the AGCM.

The NCAR CESM skillfully simulates the large-scale Australia monsoon pattern and exhibits clear improvements in the representation of intraseasonal-to-interannual variability from previous versions of this model (Meehl et al. 2012; Taschetto et al. 2011). The model captures the Australian monsoon strength and

seasonality with high fidelity compared to other climate models taking part in phases 3 and 5 of the Coupled Model Intercomparison Project (CMIP3 and CMIP5; Jourdain et al. 2013). Jourdain et al. (2013) further demonstrated that the NCAR CESM is among the 12 best CMIP3/CMIP5 models in representing the observed Australian monsoon–ENSO teleconnection. Previous studies have shown that the intensity of Australian rainfall response to El Niño and La Niña events are satisfactorily reproduced in a previous version of the NCAR model (Taschetto et al. 2010; Ummenhofer et al. 2015), although the teleconnection pattern is slightly shifted to the west (Cai et al. 2009), a common bias in CMIP5 models due to the cold tongue bias in the equatorial Pacific and a warm pool located too far west in coupled climate models (e.g., Taschetto et al. 2014).

3. Australian precipitation statistics simulated by AGCM and CPLD simulations

A brief evaluation of the model is first undertaken in terms of Australian rainfall characteristics. Figure 2 shows the annual average precipitation and seasonal averages for November–March (NDJFM) and for May–September (MJJAS) for observations and simulations. The model is able to reproduce the overall pattern and seasonality of precipitation, with increasing rainfall from the subtropics to the tropics where the monsoon occurs in DJF. However, the simulations overestimate the observed precipitation in most regions. Precipitation biases are proportionally largest in the driest regions, such as in the Australian interior. For instance, the annual observed precipitation in the Australian interior (Fig. 2a, red line) is 0.7 mm day^{-1}, while the CPLD and AGCM simulate 2.1 mm day^{-1} for the same area (i.e., approximately 3 times more rain than observed). However, it is in the tropics north of 25°S, particularly during austral summer when the monsoon occurs, that precipitation biases are largest in absolute magnitude (Figs. 2b,e,h). Elsewhere the CPLD and AGCM simulations underestimate observed rainfall over western Tasmania and along the far east coast of Australia, likely related to the inability of the model to resolve steep topography and the resulting effect on rainfall.

Despite biases in magnitude, the model broadly captures the overall spatial patterns and seasonal changes of observed precipitation over Australia. Note that the differences between observations and simulations are not overly problematic here, as the main purpose of this study is to compare the wet and dry aspects of CPLD and AGCM relative to each other. For the rest of the study, we will primarily focus on differences between the CPLD and AGCM simulations. Observations will only be evaluated when needed to put the simulated results into context with regard to historical droughts and wet spells.

Although the AGCM and CPLD simulations have the same mean state and climatology in SST by construction, they do exhibit significant differences in rainfall seasonality. In particular the absence of interannual and longer time-scale ocean variability reduces the annual mean precipitation along the northern and southern coasts of Australia but increases precipitation over the interior of Queensland, Northern Territory, and Western Australia (Fig. 2j) from November to March (Fig. 2k). The large rainfall difference in Tasmania throughout the year between AGCM and CPLD suggests that variations in SST are important for modulating rainfall. This may be linked to an enhancement of baroclinicity at the storm-track region that ultimately affects weather phenomena for southern Australia (e.g., cold fronts, cutoff lows, and blocking highs; Risbey et al. 2009).

The interannual variability of rainfall is assessed here in terms of the standard deviation of the annual mean precipitation (Figs. 3a–c). The regions where the simulated interannual standard deviation of rainfall is largest coincide with areas of larger mean rainfall (i.e., the tropics; Fig. 3a). The AGCM simulates less variability than CPLD almost everywhere (Fig. 3c), with an average reduction of 32%. This is unsurprising given the absence of variability forced by interannual oceanic changes.

The CPLD rainfall distribution is positively skewed over most of Australia (Fig. 3d). This is due in part to the nature of the precipitation distribution, which is by necessity bound below by zero but can take large positive values. The AGCM experiment has a less skewed rainfall distribution (i.e., fewer extreme heavy rainfall years) for much of the continent with the most obvious exception over the north of Australia (Fig. 3f).

The extremes of precipitation in CPLD are estimated by the 5th and 95th percentiles of annual precipitation (Figs. 3g and 3j, respectively). The AGCM simulates less intense extremes and a narrower precipitation distribution than CPLD across most of Australia, as revealed by the differences in the tails of the distribution in Figs. 3i,l.

In summary, the absence of ocean variability in the AGCM is reflected in the precipitation variability across Australia. Specifically, the CPLD experiment shows larger standard deviations and skewness and more-extreme values compared to the AGCM simulation (Figs. 3c,f,i,l).

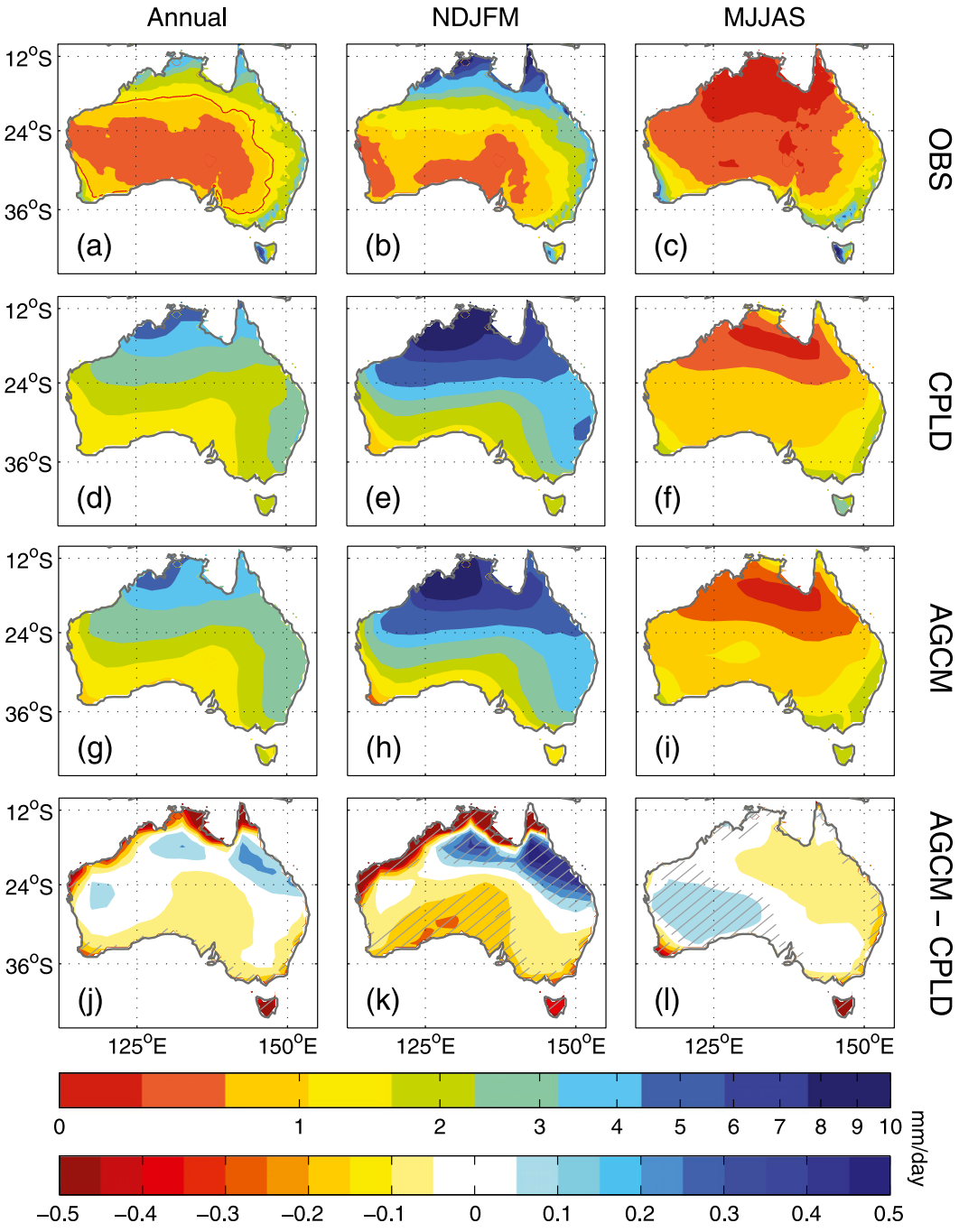

FIG. 2. Annual, NDJFM, and MJJAS averaged precipitation (mm day^{-1}). (a)–(c) Observations (OBS) from AWAP. (d)–(f) Fully coupled simulation (CPLD). (g)–(i) Atmospheric forced simulation (AGCM). (j)–(l) Differences between the AGCM and CPLD. The upper color bar refers to (a)–(i) and uses a logarithmic scale to enhance signal visibility in areas affected by the monsoon; (j)–(l) use the lower color bar. Averaged rainfall in the Australian interior delimited by the red line in (a) is quantified in the text. Gray hatching covers areas where the simulated climatologies of CPLD and AGCM differ significantly from each other at the 95% level.

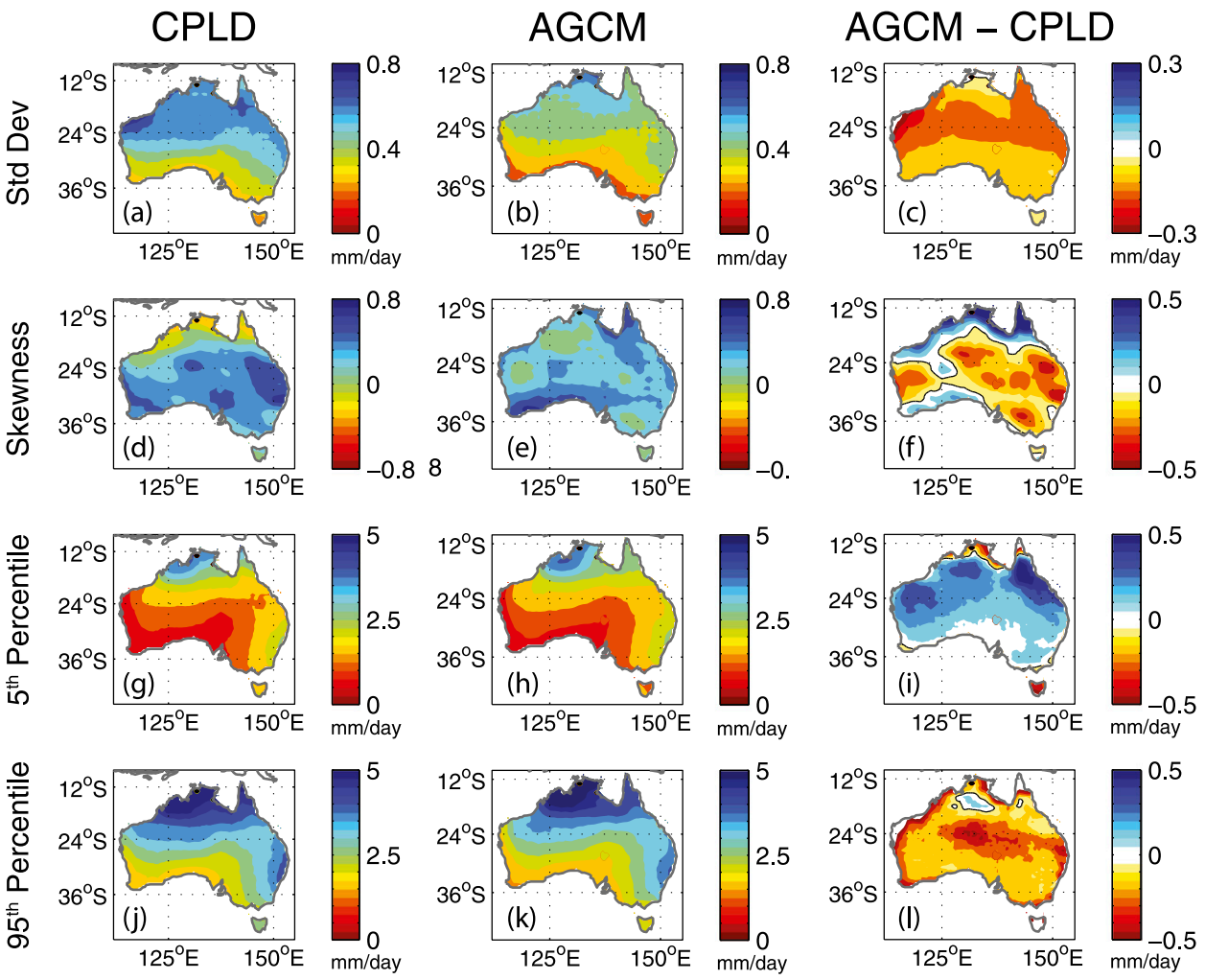

FIG. 3. (a)–(c) Standard deviation of annual precipitation over Australia (mm day^{-1}), (d)–(f) skewness of annual precipitation, calculated as the third central moment of distribution, and (g)–(i) 5th and (j)–(l) 95th percentile of annual distribution of precipitation (mm day^{-1}) for (left) CPLD, (center) AGCM, and (right) differences between the AGCM and CPLD. Black contours in the right panels represent zero.

The following sections investigate the spatial extent, duration, and intensity of simulated dry and wet periods for Australia.

4. Spatial scale of Australian dry and wet spells

We first examine whether the areal extent affected by dry and wet spells varies between CPLD and AGCM. It could be expected that droughts and wet conditions in the CPLD simulation would extend over larger areas given that coupled phenomena, such as ENSO and the IPO, are associated with large-scale reorganization of the atmospheric circulation. In contrast, the stochastic nature of internal atmospheric variability may result in more localized impacts. To address the spatial scale of rainfall extremes simulated by CPLD and AGCM, we first examine the area across Australia in which the annual rainfall exceeds the 5th and 95th percentiles (Figs. 4a–f). Note that we examine the sum of Australian land areas that experience extreme rainfall; these areas are not necessarily contiguous.

In line with our expectation, extreme wet and dry conditions simulated over Australia cover a larger area of the continent in CPLD (Figs. 4b,e) compared to the AGCM (Figs. 4c,f) simulation in most years. For instance, extreme wet (dry) conditions extending over an area exceeding one-quarter of Australia occurs 2.7 (1.5) times more frequently in CPLD than in the AGCM simulation. This means that large-scale dry/wet events are more likely to occur when coupled ocean–atmosphere variability is present.

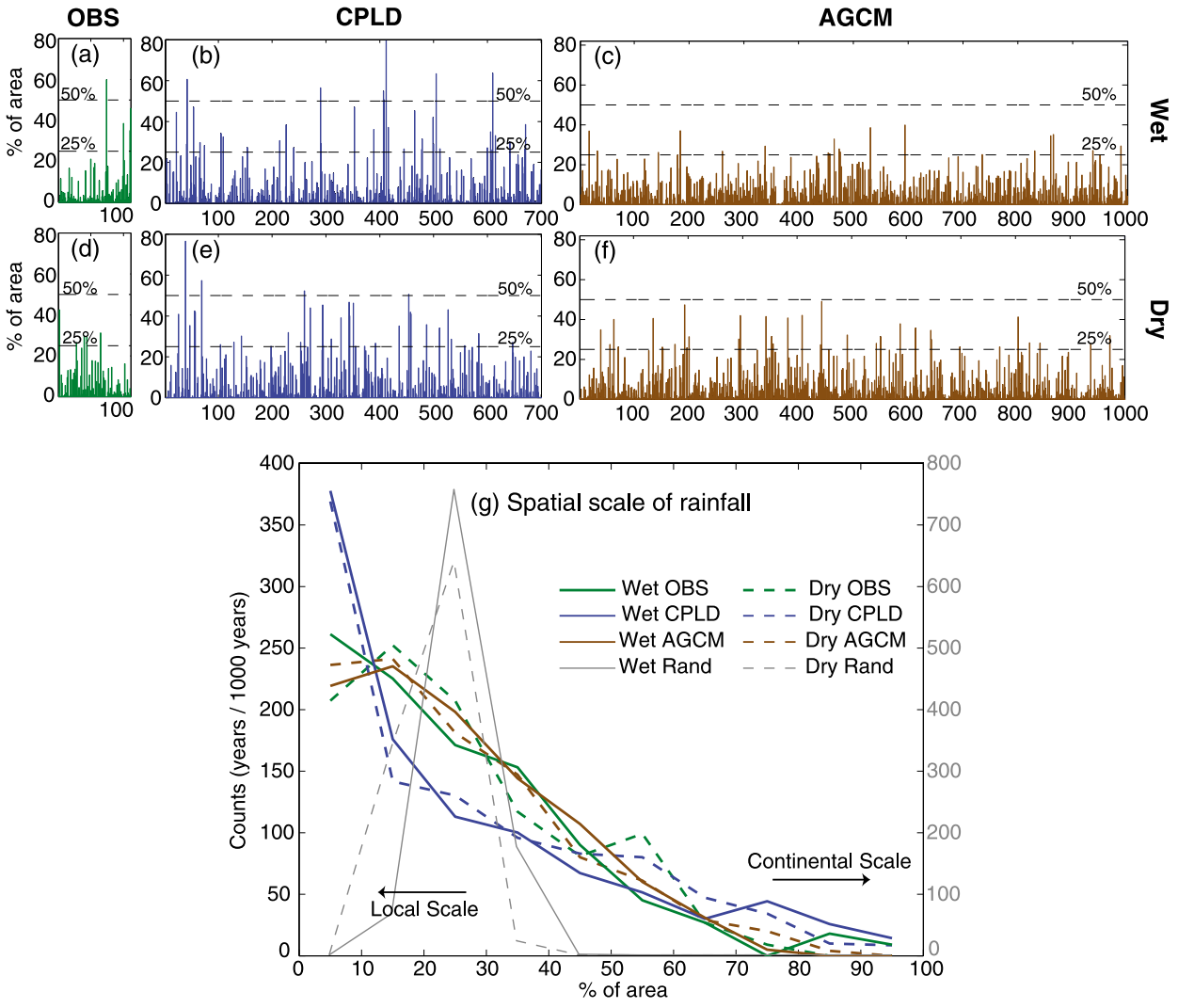

FIG. 4. Percentage of area per year in Australia where annual precipitation is (a)–(c) above the 95th percentile for a wet year and (d)–(f) below the 5th percentile for a dry year. As a reference, dashed lines in (a)–(f) represent 25% and 50% of the area. Year 100 for observations in (a),(d) represents calendar year 2000. (g) Distribution of percentage of Australian land area with annual precipitation exceeding the 75th percentile for wet years (solid lines) and with annual precipitation below the 25th percentile for dry years (dashed lines). The number of events has been normalized to 1000 years to account for the different simulation lengths. Shown are OBS (green), CPLD (blue), AGCM (brown), and uniformly distributed random values (gray). For easier visualization, the count for the random distribution is on the right *y* axis. Note that the areas exceeding the rainfall threshold are not necessarily contiguous.

In general, extreme wet conditions in observations affect a larger area of the continent than extreme dry conditions on interannual time scales (Figs. 4a,d). This asymmetry is also simulated in CPLD (Figs. 4b,e). For instance, 1% of CPLD wet events extend over 50% of the continent while only 0.5% of CPLD dry events affect more than half of Australia. Although the AGCM simulation does not show any events where extreme rainfall occurs over half of Australia, there does appear to be a significant asymmetry between the wet and dry cases (at the 90% level based on a Monte Carlo test). However, the asymmetry is in the opposite sense to that found for the CPLD experiment, with 1.9% of AGCM wet events against 3.4% of dry events affecting at least a quarter of the continental area (Figs. 4c,f).

Figure 4g shows the proportion of years when a certain percentage of the Australian land area (*x* axis) had high (solid lines; >75th percentile) or low (dashed lines; <25th percentile) rainfall. If rainfall at each grid cell were uncorrelated to neighboring grid cells, this would lead to a normal distribution of rainfall area centered around 25%. However, in the case of the model experiments, the probability of extended land areas being subject to extreme rainfall decreases for larger areas. In

particular for the CPLD experiment (Fig. 4g, blue lines), dry and wet years occur more often locally, with approximately 370 out of 1000 years affecting up to 10% of the land area. Conversely, the AGCM simulation (Fig. 4g, brown lines) shows a distribution with the maximum number of dry and wet events affecting between 10% and 20% of the area of Australia. By replacing the rainfall data with a randomly generated time series, the distribution peaks at 25% (Fig. 4g, gray lines). However, the random distribution is less concentrated around 25% if we artificially introduce a spatial autocorrelation. At a large spatial autocorrelation, the random distribution decreases monotonically (not shown) as found for the CPLD simulation in Fig. 4g. Thus, the fact that the model experiments and observations do not show peaks at 25% of the area suggests the existence of a physical mechanism (rather than a white noise process) producing coherent wet and dry patterns in both the CPLD and AGCM simulations.

The number of years when below- and above-average rainfall exceeds the 25th percentile decreases with the increase in the spatial scale (Fig. 4g). Perhaps surprisingly, the AGCM, not the CPLD, simulates a larger number of rainfall events affecting between 10% and 50% of the continent similar to observations. The difference in the number of dry and wet events affecting up to 40% of land between CPDL and AGCM is statistically different at the 95% level based on a Monte Carlo test. On the other hand, the CPLD run simulates more continental-scale impacts than the AGCM. For instance, wet (dry) events impacting over 70% of the continent occur approximately 17 (2) times more often in the CPLD than the AGCM simulation, the wet case being statistically significant at the 95% level using a Monte Carlo test (Fig. 4g). This suggests that coupled ocean–atmosphere variability plays an important role in the spatial scale of extreme rainfall events over Australia.

5. Characteristics of regional rainfall in CPLD and AGCM

As most wet and dry events simulated in Australia cover less than one-quarter of the land area, we follow the previous analysis with a regional evaluation of rainfall anomalies. Australia was initially subdivided into eight different regions, as shown in Fig. 5a (colored boxes). However, the results indicated that in the model the behavior of these regions could be largely summarized based on three main regions: 1) Western Australia (WA; 13°–35°S, 113°–129°E); 2) eastern Australia (EA; 11°–39°S, 138°–154°E), spanning Queensland, New South Wales, and Victoria; and 3) Tasmania (TAS; 40°–44°S, 143°–150°E). These regions roughly delineate the zones that are influenced by different climate modes in the surrounding oceans. Specifically, WA is primarily influenced by local processes in the Indian Ocean, EA is strongly impacted by the tropical Pacific and ENSO, and TAS is directly affected by the westerly winds and the SAM in the Southern Ocean region.

Figures 5b,d,f show the simulated climatologies of precipitation for the three selected regions. The climatologies are similar between the experiments, except for larger rainfall in CPLD than AGCM during the austral summer for WA (Fig. 5b) and EA (Fig. 5d) and throughout the year for TAS (Fig. 5f). The frequency distributions of annually averaged rainfall for all of the three regions (Figs. 5e,f) simulated in the AGCM is statistically different from CPLD at the 95% level using a Kolmogorov–Smirnov test. The annual rainfall variability estimated by the interquartile range is $0.2\,\mathrm{mm\,day^{-1}}$ larger in CPLD than AGCM for both WA and EA regions. This difference is dominated by changes in the tails of the distributions (Table 1). In contrast, the shape of the rainfall distribution for TAS remains similar in CPLD to AGCM; however, the median precipitation decreases by $0.4\,\mathrm{mm\,day^{-1}}$ in the absence of ocean variability. It is interesting that the role of the ocean for Australian rainfall seems to vary meridionally; that is, the ocean increases rainfall variability by adding extreme values to the distribution in the tropics/subtropics of Australia (i.e., WA and EA; Figs. 5c,e) but by shifting rainfall mean in the midlatitudes (i.e., TAS; Fig. 5g).

Figure 6 shows the time series of annual mean precipitation averaged for each region and the corresponding decadal time series. It is clear from the time series that rainfall anomalies simulated in CPLD are larger than in AGCM. An analysis of the standard deviation ratio between the CPLD and AGCM simulations reveals that the rainfall interannual variability due to oceanic processes is approximately 62%, 66%, and 24% larger than atmospheric variability in the WA, EA, and TAS regions, respectively. As previously discussed, the rainfall standard deviation difference between CPLD and AGCM is primarily due to more frequent extreme events for WA and EA (Fig. 5).

The power spectra and autocorrelation analyses shown in Fig. 7 reveal that AGCM rainfall variability is essentially a white noise process on interannual time scales. While autocorrelation decays exponentially in both simulations, CPLD clearly shows the enhanced memory of the coupled system for WA and EA regions. For instance, the autocorrelation coefficient crosses the zero line in 14 months for WA and EA in CPLD, similar to observations (i.e., 15 months for WA and 14 months

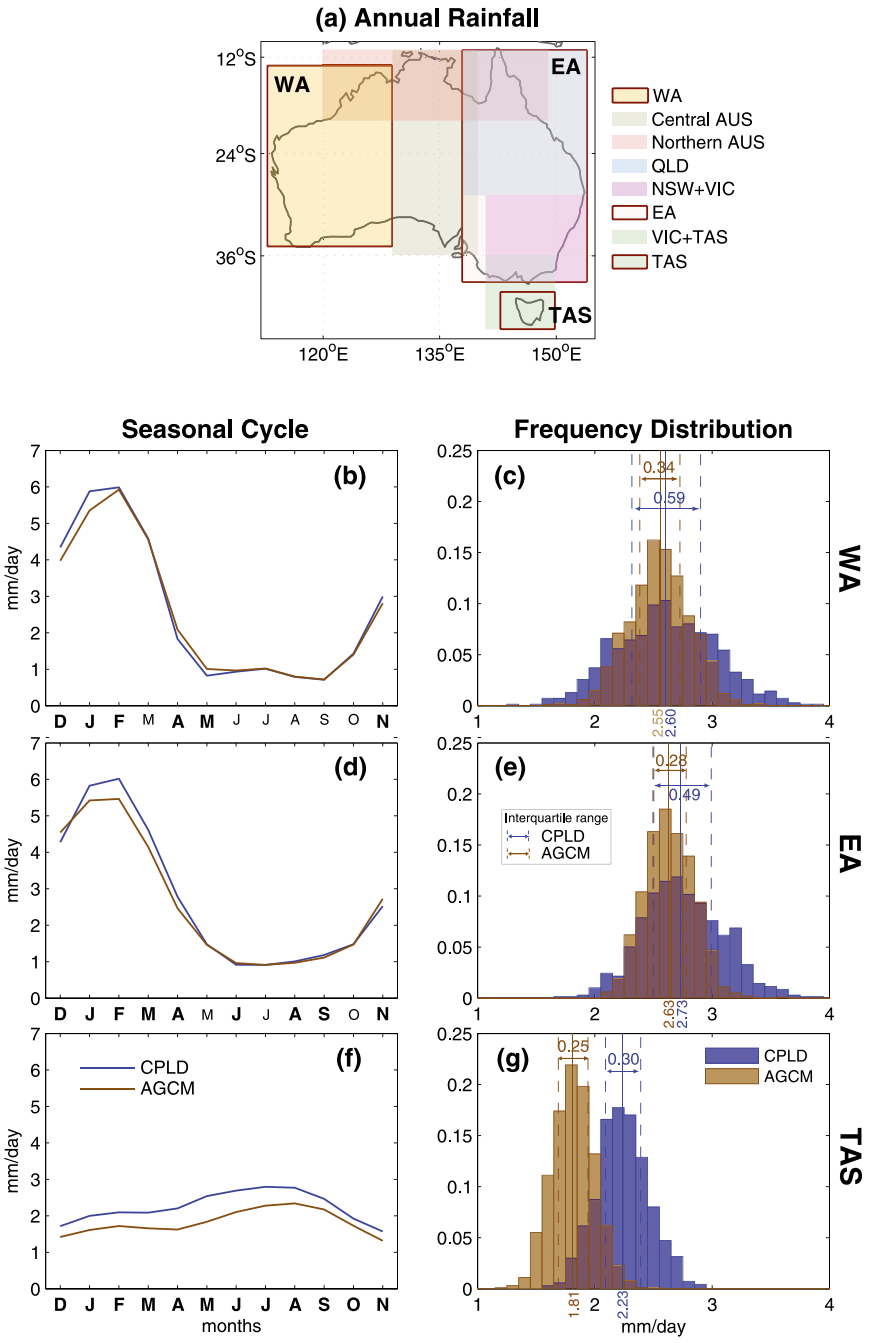

FIG. 5. (a) Shaded boxes over Australia show the areas initially used to define the selected three regions for this study (depicted by red boxes): WA, EA, and TAS. (b),(d),(f) Seasonal cycle of mean precipitation (mm day^{-1}) over the selected Australian regions for CPLD (blue line) and AGCM (brown line). Months highlighted in boldface on x axis indicate that CPLD rainfall is statistically different from the AGCM at the 95% significance level based on a Student's t test. (c),(e),(g) Probability density distributions of annual mean precipitation over the selected regions: CPLD (blue) and AGCM (brown). Interquartile ranges are specified over arrows and medians in the x axis (mm day^{-1}).

TABLE 1. Quartiles of annual mean precipitation (mm day^{-1}) in WA, EA, and TAS simulated in CPLD and AGCM and the difference between them (CPLD minus AGCM).

	25%			50%			75%		
	CPLD	AGCM	Diff	CPLD	AGCM	Diff	CPLD	AGCM	Diff
WA	2.32	2.38	−0.06	2.60	2.55	0.05	2.90	2.73	0.17
EA	2.50	2.49	0.01	2.73	2.63	0.10	2.99	2.78	0.21
TAS	2.09	1.69	0.40	2.23	1.81	0.42	2.39	1.94	0.45

for EA), while it takes 7 and 9 months for WA and EA, respectively, in AGCM (Figs. 7j,k). Curiously TAS does not show signs of additional ''memory''; that is, autocorrelation functions decay to zero in 8, 11, and 10 months in observations, CPLD, and AGCM, respectively (Fig. 7l).

While CPLD simulates larger variance concentrated within the interannual time scale of the power spectrum (Figs. 7b,e,h), the CPLD time series show larger variability concentrated with a period around 4.3 yr, particularly prominent over the WA and EA regions. This periodicity is similar to the observed 4.3 yr in WA (Fig. 7a), and it is likely associated with SST variations during ENSO and IOD events. No spectral peaks are simulated on decadal time scales in CPLD. This is consistent with previous studies that show that coupled climate models tend to underestimate the observed decadal variability particularly in the tropics (e.g., England et al. 2014).

While the AGCM power spectrum is largely flat there is some enhanced variability between 3.5 and 4 yr in WA that must be unrelated to ocean coupling (Fig. 7c). There is also a significant peak at approximately 2 yr in WA and to a lesser extent EA, possibly associated with the so-called tropospheric biennial oscillation (TBO; Meehl and Arblaster 2002). The TBO (which is thought to modulate low-latitude rainfall over Australia) has a tendency for a relatively strong Australian monsoon to be followed by a relatively weak one, and vice versa. In principle, the TBO involves coupled land–atmosphere–ocean processes over the Indo-Pacific region (Meehl and Arblaster 2002). However, a small component of TBO

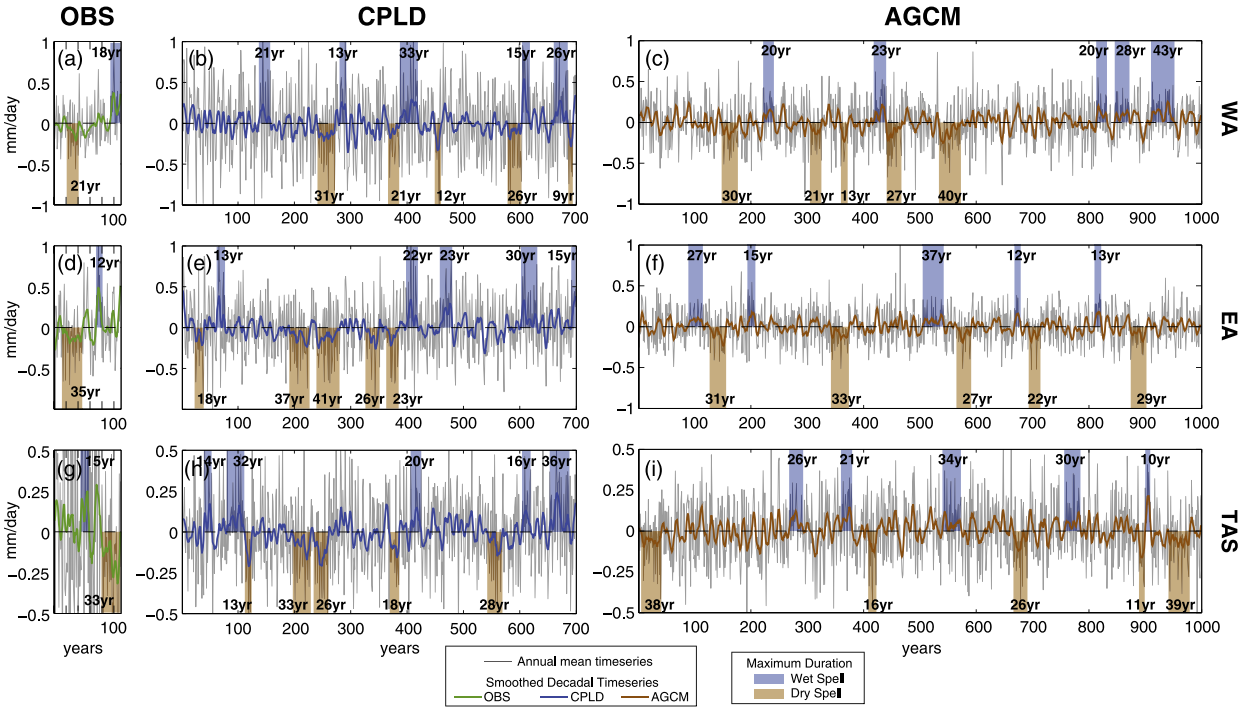

FIG. 6. Time series of mean annual rainfall (gray lines) averaged over (a)–(c) WA, (d)–(f) EA, and (g)–(i) TAS for (left) observations, (center) CPLD, and (right) AGCM simulations. To facilitate visualization, decadal variations using a smoothed time series with an 11-yr running mean window are shown in green for observations, blue for CPLD, and brown for AGCM. Shaded bars indicate the duration of the five most severe dry (brown) or wet (blue) spells in the observed (simulated) decadal time series estimated by the largest cumulative rainfall anomalies. Scale of vertical axis differs among regions.

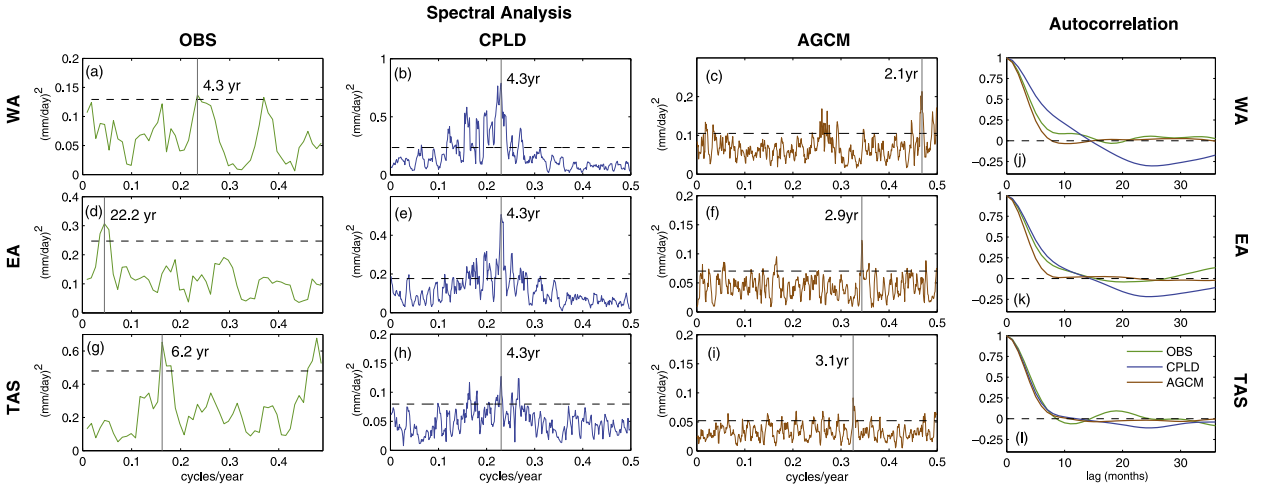

FIG. 7. Power spectrum of annual rainfall anomalies based on the multitaper method for (a),(d),(g) observations, (b),(e),(h) CPLD, and (c),(f),(i) AGCM and selected regions. The 95% confidence level based on a white noise process is shown by the black dashed line, and the vertical gray line represents the frequency of maximum power with the associated periodicity indicated next to it. Autocorrelation analysis of monthly rainfall anomalies simulated in observations (green line), CPLD (blue line), and AGCM (brown line) for (j) WA, (k) EA, and (l) TAS.

can also occur via atmosphere–land interactions only (Meehl 1994). Li et al. (2012) have shown that about half of CMIP3 and CMIP5 climate models are able to simulate TBO-like oscillations involving the ocean–atmosphere feedbacks during the Indian and Australian monsoon transitions. Here we identified no biennial peak in CPLD, only in the AGCM simulation. One may question whether the 2-yr peak is related to a physical mechanism or a statistical artifact from our power spectrum analysis. For WA it remains statistically significant at the 99% confidence level based on a white noise process.

6. Simulated intensity and duration of Australian dry/wet spells

To examine the duration of wet or dry spells, we use the averaged rainfall over the three selected regions and count the number of years when rainfall is persistently above or below average. The normalized frequency distribution for periods of multiple consecutive anomalously dry or wet years is displayed in Fig. 8. Results for each of the three selected regions are shown and plotted on a logarithmic scale in order to facilitate examination of the tails of the distributions.

To assess whether the frequency of dry or wet spells of a certain duration is different from what would be expected from a random time series, we perform a Monte Carlo test where random time series are created by reshuffling (with replacement) the simulated precipitation time series for each selected region. In this way, we compare the simulations against a random sample while preserving certain statistical properties of the original simulation, such as skewness. The resulting frequency distribution is calculated and the process is repeated 10 000 times in order to find the 95% confidence interval.

Figure 8 shows that the number of consecutive dry or wet years drops off almost exponentially. In the CPLD simulation there are significantly more 2–3-yr extreme events and significantly fewer single-year events than in the AGCM experiment. The largest change is for single-year events where the CPLD simulation has between 16% and 55% fewer individual years than in AGCM (Fig. 8). For both dry and wet conditions and for all regions the number of single-year anomalies in CPLD is statistically different from a random time series at the 95% level. The absence of ocean variability in the AGCM reduces the climatic memory provided by the ocean component and thus generates behavior that more closely matches a random distribution. In contrast, the ocean memory in CPLD tends to produce more 2–3-yr-duration dry and wet spells than expected by chance, for the WA and EA regions. For durations longer than 3 yr, somewhat surprisingly, there is no evidence that the ocean variability significantly affects the likelihood of long time-scale events (both AGCM and CPLD event frequencies are indistinguishable from a random process). Also interesting is a significant decrease in the frequency of 2-yr dry periods in WA

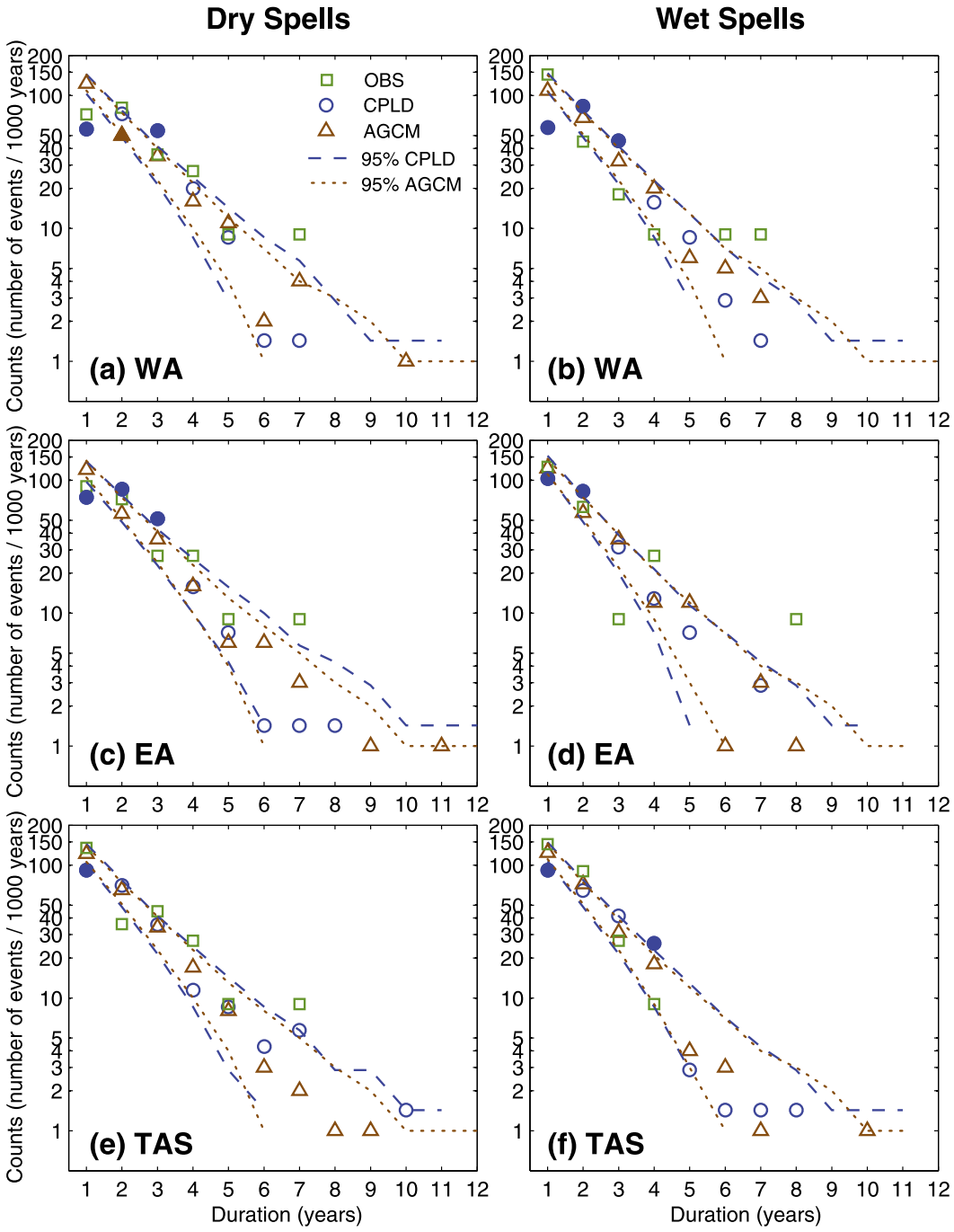

FIG. 8. Frequency distribution of (left) dry and (right) wet spells: number of events vs spell duration. To facilitate comparison, the number of events is normalized to 1000 years, and the *y* axis is a logarithmic scale. Shown are observations (squares), CPLD (circles), and AGCM (triangles). The dashed lines represent confidence levels based on the 5th and 95th percentiles of a Monte Carlo test using the simulated time series. Filled symbols are statistically significant at the 95% confidence level.

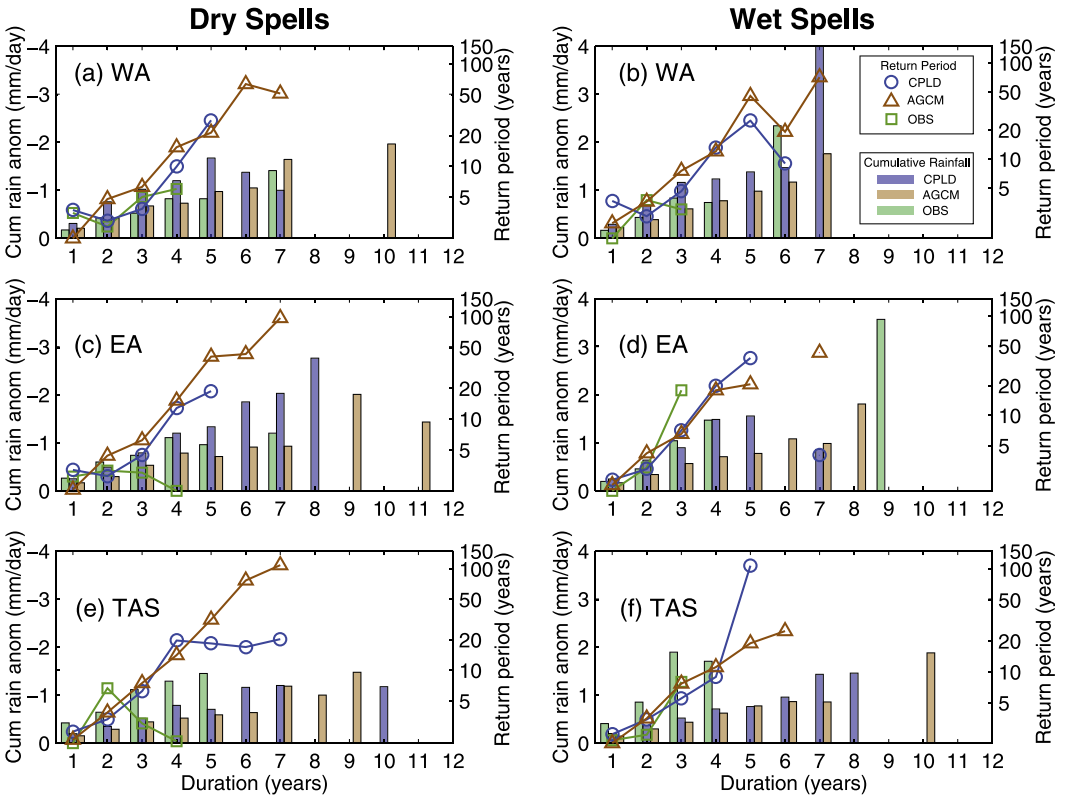

FIG. 9. Severity and return period of (left) dry and (right) wet spells with a given duration (x axis) over (a),(b) WA, (c),(d) EA, and (e),(f) TAS for observations (green), CPLD (blue), and AGCM (brown). Severity is calculated as the mean cumulative sum of averaged annual rainfall anomaly (mm day^{-1}). Return period is estimated as the mean interval (years) between the beginning of two consecutive events with a given duration. Right y axis is plotted on a logarithmic scale to facilitate visualization of events with short duration. Note that symbols and lines are discontinuous if no events are found with a given duration (refer to Fig. 8 for number of events).

simulated in the AGCM (Fig. 8a), possibly related to the 2-yr oscillation found in the AGCM power spectra (Fig. 7c).

It is interesting to see that long dry and wet spells occur not only in the CPLD run but also in the AGCM simulation. In fact the duration of dry and wet spells is essentially indistinguishable from what we expect from a random distribution, even when the ocean memory is considered. A rough statistical estimate considering a binomial distribution would give us one random chance in 1024 years of having 10 consecutive years with positive or negative rainfall [i.e., probability = $1/(2^{10})$]. Therefore, it is not surprising that both experiments simulate dry and wet spells up to a 10-yr length over the course of the around 1000-yr simulations. Durations longer than that are rare in a random sample [i.e., the 11-yr dry spell in EA simulated by AGCM (Fig. 8c) and 10-yr dry spell in TAS simulated by CPLD (Fig. 8e)]. Any comparison with observations should be made with caution as the length of the time series is about 6 (8) times shorter than CPLD (AGCM); there is therefore a much lower chance of having dry and wet spells persisting for longer than 6 years. Despite that, observations show an increased frequency of 7-yr dry and wet spells in WA and 7-yr dry and 8-yr wet spells in EA (Figs. 8a,d).

For each selected region we examine the severity and return period of dry and wet spells with different durations (Fig. 9). Regardless of the duration of the spells, dry and wet periods simulated by the CPLD simulation are more severe than for the AGCM, except for the 7-yr dry spell in WA, the 7-yr wet spell in EA, and the 5-yr wet spell in TAS. This reveals the importance of ocean variability for intensifying rainfall events over Australia. The return period of dry and wet events for TAS is similar between the two simulations. For events with a single-year duration, AGCM has a shorter return period than CPLD. Conversely, for spells with a 2–3-yr duration, AGCM produces longer return periods than CPLD. We caution comparing the return period of events longer than about 5 yr because of the limited

TABLE 2. Interannual variability and decadal-to-interannual variability ratio for observations (OBS) and simulations (CPLD and AGCM) over the selected regions. Interannual variability is calculated as the standard deviation of annual rainfall time series after removing the decadal variability. Decadal variability is calculated as the standard deviation of the 11-yr smoothed annual rainfall time series. To account for the length of the different time series, we calculate variability as the mean of 100 times the random 114-yr subperiods from the simulated rainfall time series. An error estimate for the mean variability is given as the standard deviation of the 100 random samples.

	OBS		CPLD		AGCM	
	Interannual (mm day^{-1})	Decadal-to-interannual ratio	Interannual (mm day^{-1})	Decadal-to-interannual ratio	Interannual (mm day^{-1})	Decadal-to-interannual ratio
WA	0.22	0.56	0.37 ± 0.01	0.34 ± 0.06	0.23 ± 0.02	0.44 ± 0.06
EA	0.28	0.60	0.30 ± 0.03	0.36 ± 0.05	0.18 ± 0.01	0.43 ± 0.06
TAS	0.44	0.33	0.20 ± 0.01	0.37 ± 0.04	0.16 ± 0.01	0.41 ± 0.06

sample size (see Fig. 8 for number of events with a given duration). Same caution should thus be taken for comparison with observations.

7. Decadal variability: Megadroughts and megapluvials

Multidecadal variability is simulated in both experiments, as shown in the decadal rainfall time series of Fig. 6. Decadal rainfall variability is substantially lower than interannual variability. Here we use observations to show that the decadal-to-interannual variability ratio is underestimated in the NCAR CESM model (Table 2) for all three regions. This is because simulated decadal variability is considerably smaller than in observations; that is, the values of decadal variability in the three regions range from 0.06 to 0.12 mm day^{-1} in CPLD and AGCM compared to 0.12–0.17 mm day^{-1} in observations (OBS).

The decadal variability in the simulations is comparable between CPLD and AGCM. Consequently, the decadal-to-interannual variability ratio in the AGCM is slightly larger than CPLD, given the relatively lower interannual variability in the AGCM. This is somewhat contrary to what we expect, given that intuitively the ocean memory should contribute to long-term variability in the simulations. On the other hand, we have shown previously that the ocean does not seem to affect the duration of dry and wet spells beyond around 3 yr. Therefore, we find that ocean processes in the CESM do not cause significant changes in rainfall frequency and strength at decadal time scales.

Notwithstanding the weak decadal variability in the CESM, long-term droughts and dry spells are simulated in both experiments. We highlight in Fig. 6 the most severe megadroughts and megapluvials in the smoothed time series. These are selected by calculating the periods of largest accumulated rainfall deficit and surplus for continuous dry or wet spells in the 11-yr running mean time series. The CPLD run simulates a megadrought with maximum duration of 41 yr in EA (Fig. 6e). This length is on the same order as the 39-yr megadrought in eastern Australia recently identified in paleoreconstructions by Vance et al. (2015) and associated with the IPO. The decadal time series for observations reveal a period of averaged dry conditions for about 35 yr in EA from 1913 to 1947 (Fig. 6d), a period of predominantly positive IPO. The CPLD rainfall over continental Australia is significantly correlated with the IPO in the model, with a coefficient of −0.30 in WA and −0.25 in EA. This agrees with previous studies that reported a strong modulation of Australian rainfall by the IPO using reconstruction data and twentieth-century observations (e.g., Gergis et al. 2012; Palmer et al. 2015; Power et al. 1999). The decadal rainfall time series regressed onto the SST and low-level wind anomalies (Fig. 10) supports the findings that the IPO modulates the Australian megadroughts and megapluvials in the model. This reveals a significant negative IPO pattern associated with positive rainfall in WA, in EA, and to a lesser extent in TAS (Fig. 10).

The AGCM also simulates megadroughts and megapluvials (Figs. 6c,f,i), even in the absence of ENSO and the IPO. Although the AGCM long-term events are overall less severe than the CPLD (consistent with the reduced rainfall variability due to the absence of the ocean feedback), the megadroughts and megapluvials simulated in the AGCM last as long as those in CPLD, with maximum persistence of 40 and 43 yr, respectively, in WA.

The regression pattern between the AGCM decadal rainfall time series and sea level pressure and wind anomalies shows significant variability in the eastern Indian Ocean and northern Australia for WA and EA, respectively (Figs. 11a,b). This pattern is dominant during austral summer (not shown), and it suggests that positive rainfall in both WA and EA are related to perturbations of easterly winds due to an anomalous monsoonal low in the eastern Indian

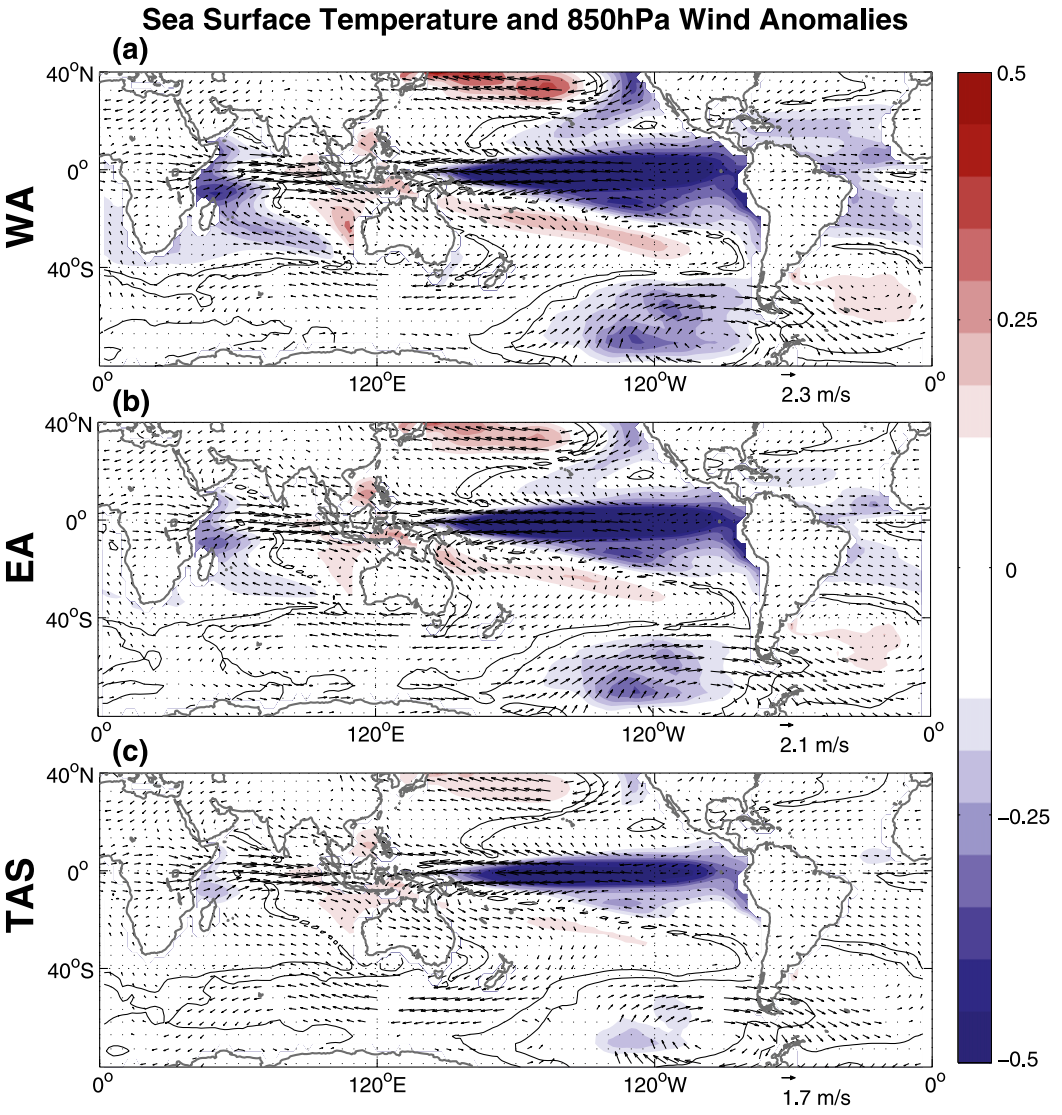

FIG. 10. CPLD rainfall time series regressed onto sea surface temperature (°C) and 850-hPa wind ($m\,s^{-1}$) anomalies for (a) WA, (b) EA, and (c) TAS. Rainfall time series are smoothed with an 11-yr running mean window. Black thin contours encompass areas statistically significant at the 95% level based on a Student's *t* test.

Ocean extending toward Western Australia. An anomalous cyclonic circulation is associated with the enhanced monsoon trough, which in turn drives northeasterly wind anomalies inland, leading to increased moisture advection and positive rainfall. For TAS (Fig. 11c), decadal variations of rainfall in the AGCM simulation is related to an anomalous low pressure center in the southern midlatitudes resembling a localized SAM pattern over the Australian sector. The reason why the SAM shows decadal excursions in the Australian sector is unclear. The SAM is a mode of variability largely intrinsic to the atmosphere and in principle has no preferred periodicity; that is, it can occur from intraseasonal to multidecadal time scales.

8. Discussion

We have found that intrinsic variability in the atmosphere–land system can drive extended periods of dry and wet episodes. This is in agreement with previous studies that reported the importance of stochastic atmospheric variability to the generation of megadroughts in many parts of the globe (Hunt 2011). We also found that ocean processes become unimportant for precipitation persistence in Australia after about three

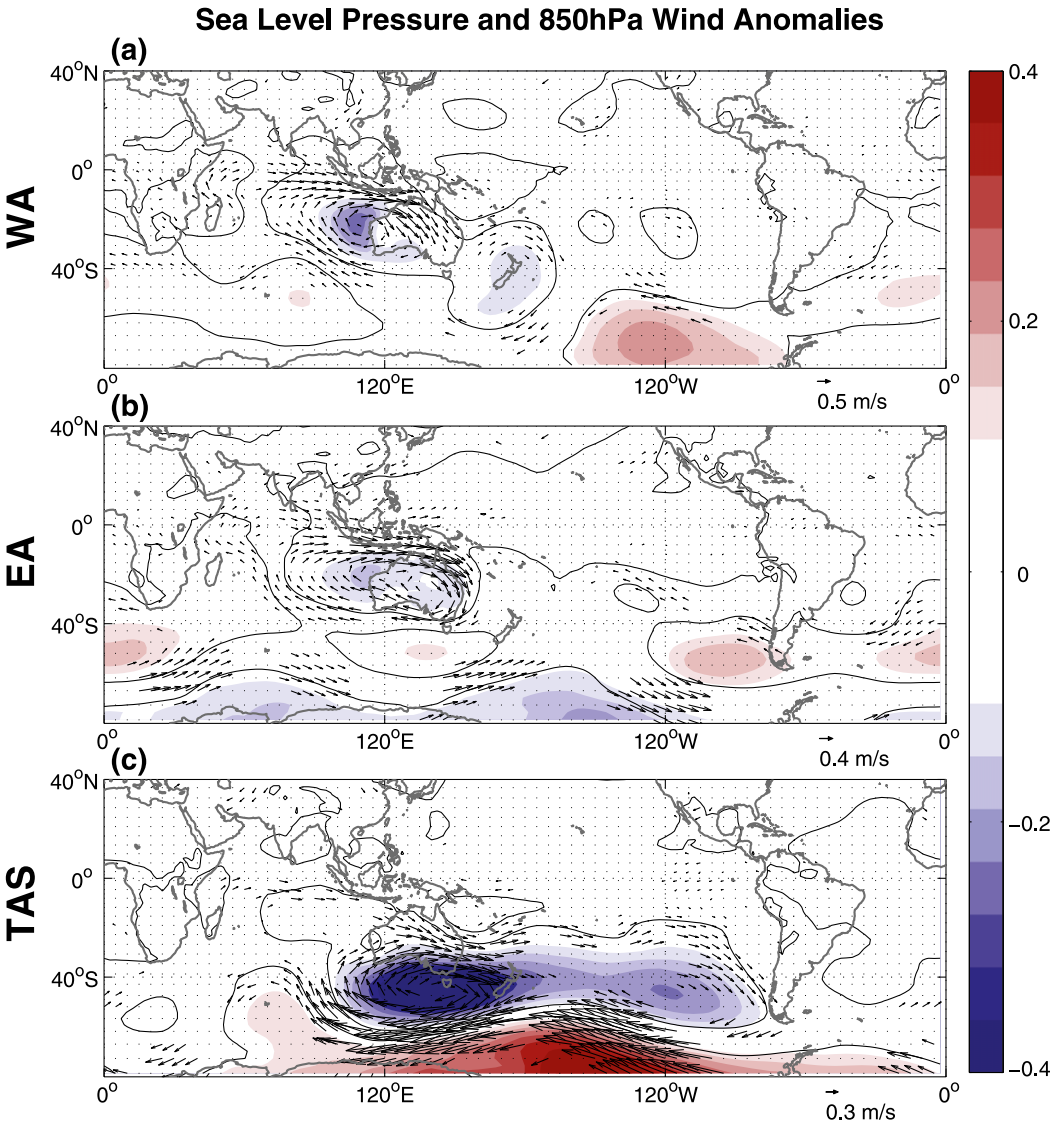

FIG. 11. AGCM rainfall time series regressed onto sea level pressure (hPa) and 850-hPa wind ($m\,s^{-1}$) anomalies for (a) WA, (b) EA, and (c) TAS. Rainfall time series are smoothed with an 11-yr running mean window. Black thin contours encompass areas statistically significant at the 95% level based on a Student's *t* test.

years. This is in agreement with findings by Boer et al. (2013), who documented a decline in potential predictability of precipitation and temperature as a result of ocean variability on interannual time scales at about 3 yr. Boer and Lambert (2008) have shown that potential predictability of precipitation then increases somewhat at longer time scales over the oceans at mid to high latitudes where the surface is connected to the deeper ocean.

One caveat here is that this is a numerical study based on a single model (i.e., the NCAR CESM). Given that climate models have considerable variability in their representation of ENSO on multidecadal-to-centennial time scales (e.g., Wittenberg 2009), as well as in atmospheric teleconnection patterns (Coats et al. 2013b), it is possible that our results are at least in part model dependent. However, the fact that previous studies have found similar results using different climate models supports our findings. For instance, using ECHAM4 and the global Hamburg Ocean Primitive Equation (ECHO-G) coupled atmosphere–ocean GCM, Coats et al. (2013a) show that stochastic atmospheric variability is able to drive persistent drought in southwestern North America. Hunt (2009) analyzed a millennium simulation with the CSIRO Mark 2 coupled global model and concluded that stochastic atmospheric processes are the cause of extensive dry periods in Australia, implying no predictability of onset, duration,

or termination of dry episodes. More recently, Stevenson et al. (2015) showed that simulated megadroughts in North America in the NCAR CESM are primarily generated by internal atmospheric variability combined with land surface coupling.

Another important aspect of our study is that our model simulations were designed to eliminate the ocean SST variability. As such, they still contain variability from the land and ice components. While sea ice is very unlikely to affect precipitation over Australia at the spatial and temporal time scales studied here, land variability can affect atmospheric circulation and thermodynamics. For example, Timbal et al. (2002) have shown that fluctuations of soil moisture increase the persistence and the variance of surface temperature and rainfall particularly over Australia. Thus, our results potentially reflect a combined effect of the atmosphere and land feedbacks on Australian dry and wet spells. Separating those effects is only possible via additional numerical simulations where land interactions are suppressed. This will be addressed in a future study.

9. Summary and conclusions

This study examines the potential role of internal atmosphere and land variability in controlling the frequency, duration, and intensity of long-term dry and wet spells over Australia. Two multicentury-scale simulations were performed with the NCAR CESM: 1) a fully coupled simulation (CPLD) and 2) an atmospheric model forced by a seasonal SST climatology derived from the coupled experiment (ACGM), such that the SST climatologies of the two experiments are identical. While CPLD contains variability from the ocean, sea ice, land, and atmosphere, the AGCM experiment eliminates fluctuations due to oceanic variability. The main results of this study can be summarized as follows.

(i) Intensity: Ocean variability makes droughts and wet spells worse. Comparison between the CPLD and AGCM simulations shows that in general interannual rainfall variability over Australia is reduced in the absence of ocean variability. The rainfall distribution in AGCM is less skewed than in CPLD over most of Australia, and dry and wet extremes in CPLD are more severe than in the AGCM. Ocean feedback processes enhance western and eastern Australia rainfall variability by about 60% compared to atmosphere-driven processes. This is mainly associated with an increase in the upper tail of the rainfall distribution. For Tasmania, the main contribution of ocean variability is to increase the mean rainfall, without affecting the variability (i.e., annual mean rainfall over TAS is around 20% larger in CPLD than AGCM). The reason why ocean feedback affects rainfall variability in continental Australia but mean rainfall in Tasmania is unclear but suggests that different mechanisms may be responsible for those differences.

(ii) Duration: Internal atmosphere- and land-forced dry and wet spells can last as long as ocean-driven events. The internal variability of the atmosphere–land system is capable of producing long periods of below- and above-average rainfall in Australia. The ocean memory has its largest impact at relatively short time scales (i.e., up to 3 yr). For time scales longer than that, ocean variability does not seem to influence the duration of wet and dry spells. We show that prolonged dry and wet spells occur not only in the CPLD but also in the AGCM; however, their durations are both indistinguishable from a random process. Power spectra analysis supports the finding that ocean memory acts around the interannual time scale range; that is, spectral energy concentrates around the 3–4-yr period, associated with ENSO events, while decadal variability cannot be distinguished from a Gaussian white noise process. This poses a challenge for long-term drought predictions for Australia.

(iii) Frequency: Internal atmosphere- and land-driven dry and wet spells occur as often as those driven by ocean processes. Overall, there is little distinction between dry and wet spell frequency in the CPLD and AGCM simulations. The clear exception is 1-yr-duration events, which occur more often in the AGCM, and the 2–3-yr-duration events, which occur more often in the CPLD run.

(iv) Spatial scale: Ocean variability plays an important role in generating large-scale rainfall impacts over Australia. Rainfall events below (above) the 25th (75th) percentile affecting over 70% of Australia occur 2 (17) times more often in the CPLD than in the AGCM simulation. Also interesting is the fact that wet spells generally tend to impact a larger area of Australia than dry spells, a feature found in the observations and simulated in the CPLD experiment. The reason for this wet and dry spatial asymmetry is unclear; however, given that this is not seen in the AGCM, it is likely to be linked with an asymmetric response of Australian rainfall to ocean modes of variability, such as El Niño and La Niña events.

(v) Multidecadal variability: Internal atmosphere–land variability is able to generate megadroughts and megapluvials. Compared to observations, decadal variability is underestimated (especially for TAS), regardless of the inclusion of ocean variability and ocean–atmosphere coupling. Despite lower intensity, the AGCM simulation generates prolonged rainfall events, or so-called megadroughts and megapluvials, with durations comparable to those of the CPLD simulation. Mega-rainfall events are primarily associated with IPO variability in the CPLD run, while in the AGCM they appear to be primarily related to perturbations in the monsoonal low and winds in the eastern Indian Ocean and northern Australia for WA and EA and to the SAM variability for TAS. Further investigation is under way to uncover the mechanisms responsible for the atmosphere-only-driven megadroughts and megapluvials.

Acknowledgments. We thank Scott Power and David Karoly for valuable feedback on this study and the reviewers and editor for their constructive comments. The use of the NCAR CESM is gratefully acknowledged. The CESM project is supported by the National Science Foundation and the Office of Science of the U.S. Department of Energy. This research was undertaken with the assistance of resources from the National Computational Infrastructure (NCI), which is supported by the Australian Government. The Australian rainfall dataset was provided by the Australian Water Availability Project. This study was supported by the Australian Research Council (ARC) under ARC-DP1094784, ARC-DP-150101331, ARC-FL100100214, and funding for C.C.U. from the National Science Foundation under AGS-1602455 and the ARC Centre of Excellence for Climate System Science.

REFERENCES

Arblaster, J. M., and G. A. Meehl, 2006: Contributions of external forcings to southern annular mode trends. *J. Climate*, **19**, 2896–2905, doi:10.1175/JCLI3774.1.

Boer, G. J., and S. J. Lambert, 2008: Multi-model decadal potential predictability of precipitation and temperature. *Geophys. Res. Lett.*, **35**, L05706, doi:10.1029/2008GL033234.

——, V. V. Kharin, and W. J. Merryfield, 2013: Decadal predictability and forecast skill. *Climate Dyn.*, **41**, 1817–1833, doi:10.1007/s00382-013-1705-0.

BoM, 2015a: Hunter Valley, February 1955. Climate education: Floods. Accessed 29 September 2015. [Available online at http://pandora.nla.gov.au/pan/96122/20090317-1643/www.bom.gov.au/lam/climate/levelthree/c20thc/flood5.html.]

——, 2015b: The big wet—January 1974. Climate education: Floods. Accessed 29 September 2015. [Available online at http://pandora.nla.gov.au/pan/96122/20090317-1643/www.bom.gov.au/lam/climate/levelthree/c20thc/flood7.html.]

Cai, W., A. Sullivan, and T. Cowan, 2009: Rainfall teleconnections with Indo-Pacific variability in the WCRP CMIP3 models. *J. Climate*, **22**, 5046–5071, doi:10.1175/2009JCLI2694.1.

——, P. van Rensch, S. Borlace, and T. Cowan, 2011: Does the southern annular mode contribute to the persistence of the multidecade-long drought over southwest Western Australia? *Geophys. Res. Lett.*, **38**, L14712, doi:10.1029/2011GL047943.

Coats, S., J. E. Smerdon, R. Seager, B. I. Cook, and J. F. González-Rouco, 2013a: Megadroughts in southwestern North America in ECHO-G millennial simulations and their comparison to proxy drought reconstructions. *J. Climate*, **26**, 7635–7649, doi:10.1175/JCLI-D-12-00603.1.

——, ——, B. I. Cook, and R. Seager, 2013b: Stationarity of the tropical Pacific teleconnection to North America in CMIP5/PMIP3 model simulations. *Geophys. Res. Lett.*, **40**, 4927–4932, doi:10.1002/grl.50938.

——, ——, ——, and ——, 2015: Are simulated megadroughts in the North American southwest forced? *J. Climate*, **28**, 124–142, doi:10.1175/JCLI-D-14-00071.1.

Cohen, T. J., and Coauthors, 2011: Continental aridification and the vanishing of Australia's megalakes. *Geology*, **39**, 167–170, doi:10.1130/G31518.1.

——, and Coauthors, 2012a: Late Quaternary mega-lakes fed by the northern and southern river systems of central Australia: Varying moisture sources and increased continental aridity. *Palaeogeogr. Palaeoclimatol. Palaeoecol.*, **356–357**, 89–108, doi:10.1016/j.palaeo.2011.06.023.

——, and Coauthors, 2012b: A pluvial episode identified in arid Australia during the medieval climatic anomaly. *Quat. Sci. Rev.*, **56**, 167–171, doi:10.1016/j.quascirev.2012.09.021.

Cook, E. R., R. Seager, M. A. Cane, and D. W. Stahle, 2007: North American drought: Reconstructions, causes, and consequences. *Earth-Sci. Rev.*, **81**, 93–134, doi:10.1016/j.earscirev.2006.12.002.

England, M. H., and Coauthors, 2014: Recent intensification of wind-driven circulation in the Pacific and the ongoing warming hiatus. *Nat. Climate Change*, **4**, 222–227, doi:10.1038/nclimate2106.

Feng, X., T. DelSole, and P. Houser, 2011: Bootstrap estimated seasonal potential predictability of global temperature and precipitation. *Geophys. Res. Lett.*, **38**, L07702, doi:10.1029/2010GL046511.

Gallant, A. J. E., S. J. Phipps, D. J. Karoly, A. B. Mullan, and A. M. Lorrey, 2013: Nonstationary Australasian teleconnections and implications for paleoclimate reconstructions. *J. Climate*, **26**, 8827–8849, doi:10.1175/JCLI-D-12-00338.1.

Gent, P. R., and Coauthors, 2011: The Community Climate System Model version 4. *J. Climate*, **24**, 4973–4991, doi:10.1175/2011JCLI4083.1.

Gergis, J., and Coauthors, 2012: On the long-term context of the 1997–2009 ''Big Dry'' in south-eastern Australia: Insights from a 206-year multi-proxy rainfall reconstruction. *Climatic Change*, **111**, 923–944, doi:10.1007/s10584-011-0263-x.

Hendon, H. H., D. W. J. Thompson, and M. C. Wheeler, 2007: Australian rainfall and surface temperature variations associated with the Southern Hemisphere annular mode. *J. Climate*, **20**, 2452–2467, doi:10.1175/JCLI4134.1.

——, E.-P. Lim, J. M. Arblaster, and D. L. T. Anderson, 2014: Causes and predictability of the record wet east Australian spring 2010. *Climate Dyn.*, **42**, 1155–1174, doi:10.1007/s00382-013-1700-5.

Hill, K. J., A. Santoso, and M. H. England, 2009: Interannual Tasmanian rainfall variability associated with large-scale climate modes. *J. Climate*, **22**, 4383–4397, doi:10.1175/2009JCLI2769.1.

Hunt, B. G., 2009: Multi-annual dry episodes in Australian climatic variability. *Int. J. Climatol.*, **29**, 1715–1730, doi:10.1002/joc.1820.

——, 2011: Global characteristics of pluvial and dry multi-year episodes, with emphasis on megadroughts. *Int. J. Climatol.*, **31**, 1425–1439, doi:10.1002/joc.2166.

——, 2012: Stochastic control of Indian megadroughts and megafloods. *Climate Dyn.*, **39**, 1801–1821, doi:10.1007/s00382-012-1392-2.

Jourdain, N. C., A. Sen Gupta, A. S. Taschetto, C. C. Ummenhofer, A. F. Moise, and K. Ashok, 2013: The Indo-Australian monsoon and its relationship to ENSO and IOD in reanalysis data and the CMIP3/CMIP5 simulations. *Climate Dyn.*, **41**, 3073–3102, doi:10.1007/s00382-013-1676-1.

——, M. Lengaigne, J. Vialard, T. Izumo, and A. Sen Gupta, 2016: Further insights on the influence of the Indian Ocean dipole on the following year's ENSO from observations and CMIP5 models. *J. Climate*, **29**, 637–658, doi:10.1175/JCLI-D-15-0481.1.

Karoly, D., J. Risbey, and A. Reynolds, 2003: Global warming contributes to Australia's worst drought. World Wide Fund for Nature Rep., 8 pp.

Kiem, A. S., and D. C. Verdon-Kidd, 2010: Towards understanding hydroclimatic change in Victoria, Australia—Preliminary insights into the "Big Dry." *Hydrol. Earth Syst. Sci.*, **14**, 433–445, doi:10.5194/hess-14-433-2010.

Kushnir, Y., W. A. Robinson, I. Bladé, N. M. J. Hall, S. Peng, and R. Sutton, 2002: Atmospheric GCM response to extratropical SST anomalies: Synthesis and evaluation. *J. Climate*, **15**, 2233–2256, doi:10.1175/1520-0442(2002)015<2233:AGRTES>2.0.CO;2.

Li, Y., N. C. Jourdain, A. S. Taschetto, C. C. Ummenhofer, K. Ashok, and A. Sen Gupta, 2012: Evaluation of monsoon seasonality and the tropospheric biennial oscillation transitions in the CMIP models. *Geophys. Res. Lett.*, **39**, L20713, doi:10.1029/2012GL053322.

Lim, E.-P., H. H. Hendon, and H. Rashid, 2013: Seasonal predictability of the southern annular mode due to its association with ENSO. *J. Climate*, **26**, 8037–8054, doi:10.1175/JCLI-D-13-00006.1.

——, ——, J. M. Arblaster, C. Chung, A. F. Moise, P. Hope, G. Young, M. Zhao, 2016: Interaction of the recent 50 year SST trend and La Niña 2010: Amplification of the southern annular mode and Australian springtime rainfall. *Climate Dyn.*, doi:10.1007/s00382-015-2963-9, in press.

Manabe, S., and R. J. Stouffer, 1996: Low-frequency variability of surface air temperature in a 1000-year integration of a coupled atmosphere–ocean–land surface model. *J. Climate*, **9**, 376–393, doi:10.1175/1520-0442(1996)009<0376:LFVOSA>2.0.CO;2.

Meehl, G. A., 1994: Influence of the land surface in the Asian summer monsoon: External conditions versus internal feedbacks. *J. Climate*, **7**, 1033–1049, doi:10.1175/1520-0442(1994)007<1033:IOTLSI>2.0.CO;2.

——, and J. M. Arblaster, 2002: The tropospheric biennial oscillation and Asian–Australian monsoon rainfall. *J. Climate*, **15**, 722–744, doi:10.1175/1520-0442(2002)015<0722:TTBOAA>2.0.CO;2.

——, ——, J. M. Caron, H. Annamalai, M. Jochum, A. Chakraborty, and R. Murtugudde, 2012: Monsoon regimes and processes in CCSM4. Part I: The Asian–Australian monsoon. *J. Climate*, **25**, 2583–2608, doi:10.1175/JCLI-D-11-00184.1.

——, and Coauthors, 2014: Decadal climate prediction: An update from the trenches. *Bull. Amer. Meteor. Soc.*, **95**, 243–267, doi:10.1175/BAMS-D-12-00241.1.

Meinke, H., P. deVoil, G. L. Hammer, S. Power, R. Allan, R. C. Stone, C. Folland, and A. Potgieter, 2005: Rainfall variability at decadal and longer time scales: Signal or noise? *J. Climate*, **18**, 89–96, doi:10.1175/JCLI-3263.1.

Nicholls, N., 2004: The changing nature of Australian droughts. *Climatic Change*, **63**, 323–336, doi:10.1023/B:CLIM.0000018515.46344.6d.

——, W. Drosdowsky, and B. Lavery, 1997: Australian rainfall variability and change. *Weather*, **52**, 66–72, doi:10.1002/j.1477-8696.1997.tb06274.x.

Okumura, Y. M., and C. Deser, 2010: Asymmetry in the duration of El Niño and La Niña. *J. Climate*, **23**, 5826–5843, doi:10.1175/2010JCLI3592.1.

Palmer, J. G., and Coauthors, 2015: Drought variability in the eastern Australia and New Zealand summer drought atlas (ANZDA, CE 1500–2012) modulated by the interdecadal Pacific oscillation. *Environ. Res. Lett.*, **10**, 124002, doi:10.1088/1748-9326/10/12/124002.

Power, S., F. Tseitkin, M. Dix, R. Kleeman, R. Colman, and D. Holland, 1995: Stochastic variability at the air–sea interface on decadal timescales. *Geophys. Res. Lett.*, **22**, 2593–2596, doi:10.1029/95GL02655.

——, T. Casey, C. Folland, A. Colman, and V. Mehta, 1999: Inter-decadal modulation of the impact of ENSO on Australia. *Climate Dyn.*, **15**, 319–324, doi:10.1007/s003820050284.

——, M. Haylock, R. Colman, and X. Wang, 2006: The predictability of interdecadal changes in ENSO activity and ENSO teleconnections. *J. Climate*, **19**, 4755–4771, doi:10.1175/JCLI3868.1.

Raupach, M. R., P. R. Briggs, V. Haverd, E. A. King, M. Paget, and C. M. Trudinger, 2009: Australian water availability project (AWAP): CSIRO marine and atmospheric research component: Final report for phase 3. CAWCR Tech. Rep. 013, 67 pp. [Available online at http://www.csiro.au/awap/doc/CTR_013_online_FINAL.pdf.]

Risbey, J. S., M. J. Pook, P. C. McIntosh, M. C. Wheeler, and H. H. Hendon, 2009: On the remote drivers of rainfall variability in Australia. *Mon. Wea. Rev.*, **137**, 3233–3253, doi:10.1175/2009MWR2861.1.

Rowell, D. P., 1998: Assessing potential seasonal predictability with an ensemble of multidecadal GCM simulations. *J. Climate*, **11**, 109–120, doi:10.1175/1520-0442(1998)011<0109:APSPWA>2.0.CO;2.

Sen Gupta, A., and M. England, 2006: Coupled ocean–atmosphere–ice response to variations in the southern annular mode. *J. Climate*, **19**, 4457–4486, doi:10.1175/JCLI3843.1.

——, and ——, 2007: Coupled ocean–atmosphere feedback in the southern annular mode. *J. Climate*, **20**, 3677–3692, doi:10.1175/JCLI4200.1.

Seviour, W. J. M., S. C. Hardiman, L. J. Gray, N. Butchart, C. MacLachlan, and A. A. Scaife, 2014: Skillful seasonal prediction of the southern annular mode and Antarctic ozone. *J. Climate*, **27**, 7462–7474, doi:10.1175/JCLI-D-14-00264.1.

Shukla, J., 1981: Dynamical predictability of monthly means. *J. Atmos. Sci.*, **38**, 2547–2572, doi:10.1175/1520-0469(1981)038<2547:DPOMM>2.0.CO;2.

——, and Coauthors, 2000: Dynamical seasonal prediction. *Bull. Amer. Meteor. Soc.*, **81**, 2593–2606, doi:10.1175/1520-0477(2000)081<2593:DSP>2.3.CO;2.

Stevenson, S., A. Timmermann, Y. Chikamoto, S. Langford, and P. DiNezio, 2015: Stochastically generated North American

megadroughts. *J. Climate*, **28**, 1865–1880, doi:10.1175/JCLI-D-13-00689.1.

Taschetto, A. S., and I. Wainer, 2008: Reproducibility of South American precipitation due to subtropical South Atlantic SSTs. *J. Climate*, **21**, 2835–2851, doi:10.1175/2007JCLI1865.1.

——, R. J. Haarsma, A. Sen Gupta, C. C. Ummenhofer, K. J. Hill, and M. H. England, 2010: Australian monsoon variability driven by a Gill–Matsuno-type response to central west Pacific warming. *J. Climate*, **23**, 4717–4736, doi:10.1175/2010JCLI3474.1.

——, A. Sen Gupta, H. H. Hendon, C. C. Ummenhofer, and M. H. England, 2011: The contribution of Indian Ocean sea surface temperature anomalies on Australian summer rainfall during El Niño events. *J. Climate*, **24**, 3734–3747, doi:10.1175/2011JCLI3885.1.

——, ——, N. C. Jourdain, A. Santoso, C. C. Ummenhofer, and M. H. England, 2014: Cold tongue and warm pool ENSO events in CMIP5: Mean state and future projections. *J. Climate*, **27**, 2861–2885, doi:10.1175/JCLI-D-13-00437.1.

Timbal, B., S. Power, R. Colman, J. Viviand, and S. Lirola, 2002: Does soil moisture influence climate variability and predictability over Australia? *J. Climate*, **15**, 1230–1238, doi:10.1175/1520-0442(2002)015<1230:DSMICV>2.0.CO;2.

Ummenhofer, C. C., M. H. England, P. C. McIntosh, G. A. Meyers, M. J. Pook, J. S. Risbey, A. Sen Gupta, and A. S. Taschetto, 2009: What causes southeast Australia's worst droughts? *Geophys. Res. Lett.*, **36**, L04706, doi:10.1029/2008GL036801.

——, and Coauthors, 2011: Indian and Pacific Ocean influences on southeast Australian drought and soil moisture. *J. Climate*, **24**, 1313–1336, doi:10.1175/2010JCLI3475.1.

——, A. Sen Gupta, M. H. England, A. S. Taschetto, P. R. Briggs, and M. R. Raupach, 2015: How did ocean warming affect Australian rainfall extremes during the 2010/2011 La Niña event? *Geophys. Res. Lett.*, **42**, 9942–9951, doi:10.1002/2015GL065948.

Vance, T. R., J. L. Roberts, C. T. Plummer, A. S. Kiem, and T. D. van Ommen, 2015: Interdecadal Pacific variability and eastern Australian megadroughts over the last millennium. *Geophys. Res. Lett.*, **42**, 129–137, doi:10.1002/2014GL062447.

Verdon-Kidd, D. C., and A. S. Kiem, 2009: Nature and causes of protracted droughts in southeast Australia: Comparison between the Federation, WWII, and Big Dry Droughts. *Geophys. Res. Lett.*, **36**, L22707, doi:10.1029/2009GL041067.

Wittenberg, A. T., 2009: Are historical records sufficient to constrain ENSO simulations? *Geophys. Res. Lett.*, **36**, L12702, doi:10.1029/2009GL038710.